Surface and Reduction Energetics of the CeO_2-ZrO_2 Catalysts

Gabriele Balducci,* Jan Kašpar, Paolo Fornasiero, and Mauro Graziani

Universita' degli Studi di Trieste, Dipartimento di Scienze Chimiche, via L.Giorgieri 1, 34127 Trieste, Italy

M. Saiful Islam

Department of Chemistry, University of Surrey, Guildford, Surrey GU2 5XH, U.K.

Received: July 23, 1997; In Final Form: October 25, 1997[⊗]

The (110), (111), and (310) surfaces of cubic CeO_2-ZrO_2 solid solutions have been studied by computer simulation techniques using atomistic models. Surface energies, Ce^{4+}/Ce^{3+} reduction energies, and penetration profiles of oxygen vacancy formation have been calculated. The results of the calculations suggest some possible factors that could explain the increase in the oxygen storage capacity experimentally observed in these systems relative to pure ceria: surface Ce^{4+}/Ce^{3+} reduction energies are comparable with previously found bulk values; introduction of zirconia into the ceria lattice decreases the Ce^{4+}/Ce^{3+} reduction energy on the stable (110) and (111) surfaces; oxygen vacancies tend to segregate to these surfaces.

Introduction

Ceria (CeO_2) is being widely used as an additive in catalytic systems for the elimination of the pollutants contained in the exhaust gases of automobiles.[1] Oxygen storage capacity, due to a facile $Ce^{4+} \rightleftharpoons Ce^{3+}$ interconversion,[2] improvement of the noble metal catalyst dispersion,[3] surface area stabilization of the alumina support,[4] promotion of the water gas shift reaction,[3] and direct interaction with the noble metal particles[5] are among the recognized functions of this material. Of particular relevance is the ability to act as a chemical air-to-fuel ratio regulator, due to the facile reaction

$$2CeO_2 \rightleftharpoons Ce_2O_3 + {}^1/_2O_2 \qquad (1)$$

which consumes and releases oxygen under "lean" and "rich" mixture conditions, respectively. Three-way catalysts can achieve an acceptable simultaneous conversion of the three main pollutants found in automobile emissions (i.e., CO, NO_x, and hydrocarbons) only when the air-to-fuel ratio is very close to its stoichiometric value,[1] hence, the importance of reaction 1 as a stabilizing factor of the catalyst activity. Recently, it was found experimentally that incorporation of zirconia (ZrO_2) into ceria to form a solid solution gives a material in which the reducibility of Ce^{4+} is greatly enhanced:[6,7] reduction peaks at about 700 K have been observed during temperature-programmed reduction experiments.[7,8] In these experiments, it was possible to assess unambiguously the participation of a large fraction of the bulk material in the reduction process. In an effort to clarify the mechanism through which zirconia brings about an improved Ce^{4+} reducibility in the solid solutions, we studied the energetics of the $Ce^{4+} \rightarrow Ce^{3+}$ reaction and the related oxygen vacancy formation in the bulk material by computer simulation techniques.[9] It is found that the bulk reduction energy is reduced significantly even by small amounts of zirconia. It is clear that the redox process must also involve the surface of the mixed oxide. Moreover, the surface of the solid solutions differs in varying degree from the bulk, and this is expected to affect to some extent the energy changes associated with the redox process. These considerations prompted us to extend our recent bulk simulations[9] to the modeling of the surfaces of CeO_2-ZrO_2 solid solutions, with particular emphasis on those aspects related to the Ce^{4+}/Ce^{3+} redox behavior. While we are unaware of any previous computational study on the mixed CeO_2-ZrO_2 system, a number of papers have focused on the two single components CeO_2[10−15] and ZrO_2.[16−20] In the present work we present surface energy calculations as well as Ce^{4+}/Ce^{3+} reduction and oxygen vacancy surface segregation energies for the (110), (111), and (310) surfaces of cubic CeO_2-ZrO_2 solid solutions in the whole composition range.

Computational Methods

The computational methodologies for the atomistic simulation of the surfaces of ionic materials are well established[21,22] and will only be outlined here. The simulations are formulated within the framework of the Born model, in which the ionic species are assigned integer charges corresponding to their formal oxidation states. Each ion interacts with all others through a pair potential consisting of a long-range Coulombic component and a short-range term, which in the present work has the form of a Buckingham function:

$$E_{\text{short range}} = A \exp\left(-\frac{r}{\rho}\right) - \frac{C}{r^6} \qquad (2)$$

A cutoff of 1.5a (a being the lattice constant) was used for the short-range potential. Each ion is allowed to undergo polarization due to the electric field produced by all others. This is achieved by the use of the shell model,[23] which represents each ion as a massless shell with charge Y connected to an inner core through a harmonic potential of the form

$$E_{\text{core-shell}} = {}^1/_2 k_2 d^2 \qquad (3)$$

where k_2 is a force constant and d is the relative displacement

* Corresponding author. E-mail: balducci@univ.trieste.it.

⊗ Abstract published in *Advance ACS Abstracts,* December 15, 1997.

S1089-5647(97)02400-0 CCC: $15.00
Published on Web 01/15/1998

TABLE 1: Potential Parameters Employed in the Present Work[a]

Short-Range Potential Parameters: $V(r) = A\exp(-r/\rho) - C/r^6$			
	A (eV)	ρ (Å)	C (eV Å^6)
$O^{2-}-O^{2-}$	22764.30	0.1490	27.89
$Zr^{4+}-O^{2-}$	985.87	0.3760	0.00
$Ce^{4+}-O^{2-}$	1986.83	0.3511	20.40
$Ce^{3+}-O^{2-}$	1731.62	0.3637	14.43

Shell Model Parameters: $V(r) = k_2r^2$		
	shell charge (e)	k_2 (eV Å^{-2})
O^{2-}	−2.08	27.29
Zr^{4+}	1.35	169.62
Ce^{4+}	7.70	291.75
Ce^{3+}	7.70	291.75

[a] The Zr^{4+} and O^{2-} parameters are taken from the paper on CaO-doped zirconia by Dwivedi and Cormack;[17] Ce^{4+} and Ce^{3+} potentials are those employed by Sayle *et al.* for modeling bulk and surface defects in pure ceria.[12]

of the core and shell. The core charge is determined so that the total charge of the shell plus core system equals the integral charge value of the ionic species. Coupling between short-range forces and ionic polarizability is achieved by allowing the short-range potentials to act only between shell species. With the above analytical expressions the lattice energy can be evaluated and minimized with respect to the ionic coordinates. The potential parameters employed in the present paper (Table 1) are the same as those used in our previous work[9] and produce good agreement between simulated and observed cell constants across the whole composition range.

Surface energies are evaluated according to

$$\gamma = \frac{E_S - {}^1/_2E_B}{A} \tag{4}$$

where E_S is the energy of a surface-terminated crystal block, E_B is the energy of two crystal blocks put together so that they match (thus E_B is the energy of the bulk crystal and must be divided by two to be compared to E_S, since the number of atoms considered in its calculation is twice that considered in the calculation of E_S), and A is the surface area. This calculation was performed using the computer code MIDAS.[24] One crucial point about the surface energy calculations is the relaxation of ions near the surface, as a consequence of the abrupt interruption of the perfect lattice periodicity. This is achieved by considering the crystal as a stack of planes with 2D periodicity. The stack is divided into two regions: in the first one, which terminates on the surface, ions are individually relaxed, while in the second region ions preserve their mutual positions, but the whole region can move relative to the first, thus providing the correct potential for the ions at the bottom of the first region. The energy of a surface defect is evaluated through a two-region approach,[25,26] suitably adapted to account for the presence of the surface and implemented in the CHAOS code.[27] The perfect relaxed surface constitutes the starting point for the defect calculation. The crystal around the surface defect is divided into two hemispherical and concentric regions. All the atoms in the inner region are individually relaxed under the perturbation produced by the defect, while the displacements and polarization of the ions in the outer region can be evaluated using simplified formulas derived from the macroscopic dielectric constant,[25] owing to their larger distance from the perturbation origin. The inner region contained typically 100 atoms, while the size of the outer region was adjusted so that it could include the effect of the short-range interactions between the ions on the boundary (but within) the inner region and all the ions in the outer region. As with our previous bulk simulations, the different compositions of the CeO_2-ZrO_2 solid solution have been simulated using a mean field approach: the $Ce_xZr_{(1-x)}O_2$ system is assumed to contain a single cationic species, hybrid between Ce^{4+} and Zr^{4+}. Accordingly, the short-range interaction between the hybrid cation M^{4+} and the oxide ion can be expressed as

$$\begin{aligned} E_{M^{4+}-O^{2-}} &= xE_{Ce^{4+}-O^{2-}} + (1-x)E_{Zr^{4+}-O^{2-}} \\ &= xA_{Ce^{4+}-O^{2-}}\exp\left(-\frac{r}{\rho_{Ce^{4+}-O^{2-}}}\right) + \\ &\quad (1-x)A_{Zr^{4+}-O^{2-}}\exp\left(-\frac{r}{\rho_{Zr^{4+}-O^{2-}}}\right) - \\ &\quad \frac{xC_{Ce^{4+}-O^{2-}} + (1-x)C_{Zr^{4+}-O^{2-}}}{r^6} \end{aligned} \tag{5}$$

x being the CeO_2 molar fraction. Owing to the use of mean field potentials, a correction had to be applied to take into account the transformation of hybrid M^{4+} cations into "pure" Ce^{4+} species, according to

$$E_{Ce^{4+}\rightarrow Ce^{3+}} = E_{M^{4+}\rightarrow Ce^{3+}} - E_{M^{4+}\rightarrow Ce^{4+}} \tag{6}$$

A cubic fluorite structure was assumed for the solid solutions at all compositions, since the most important experimental results in terms of enhanced Ce^{4+}/Ce^{3+} reducibility have been obtained with materials of this structure.[6,7] However, we are aware that, especially for the higher zirconia contents, CeO_2-ZrO_2 solid solutions often present a tetragonal structure.[28,29]

Results and Discussion

Surface Structures. The (110) and (310) surfaces of the fluorite structure are classified as "type 1" surfaces:[30] they contain stoichiometric amounts of cations and anions in each plane and thus are electrically neutral. On the other hand, the (111) surface is of "type 2"; i.e., along the normal to the surface a sequence of charged planes is found, the repeating unit consisting of a neutral $[O^{2-}-M^{4+}-O^{2-}]$ slab. Both types of surfaces are predicted to be stable since they have no net dipole moment perpendicular to the surface.[30] In Figure 1 the surface energy calculations for the perfect surfaces of the CeO_2-ZrO_2 solid solutions considered in this work are reported, both before and after relaxation. It is clear that the surface energies corresponding to the fully relaxed structures are lower than those for the unrelaxed structures. This emphasizes the importance of treating surface relaxation effects and that models of catalytic processes based on ideal (unrelaxed) surface structures may have serious flaws. As a representative example, the three surface structures of $Ce_{0.5}Zr_{0.5}O_2$, both before and after relaxation, are shown in Figure 2.

We were unable to find in the literature any experimental surface energy determination for the mixed CeO_2-ZrO_2 oxide for direct comparison. However, our surface energies for pure ceria ($Ce_xZr_{(1-x)}O_2$ with $x = 1.0$) are in accord with previously published calculations.[12,14] On the pure zirconia side of the mixed oxide system ($Ce_xZr_{(1-x)}O_2$ with $x = 0.0$) the relaxed energies for the (110), (111), and (310) surfaces (2.10, 1.19, and 2.31 J/m^2, respectively) compare well with the experimental average value extrapolated to 0 K of 1.428 J/m^2, which was determined with the multiphase equilibration technique in cubic calcia stabilized zirconia.[31] From Figure 1 it is seen that the (111) surface is the most stable at all compositions and will

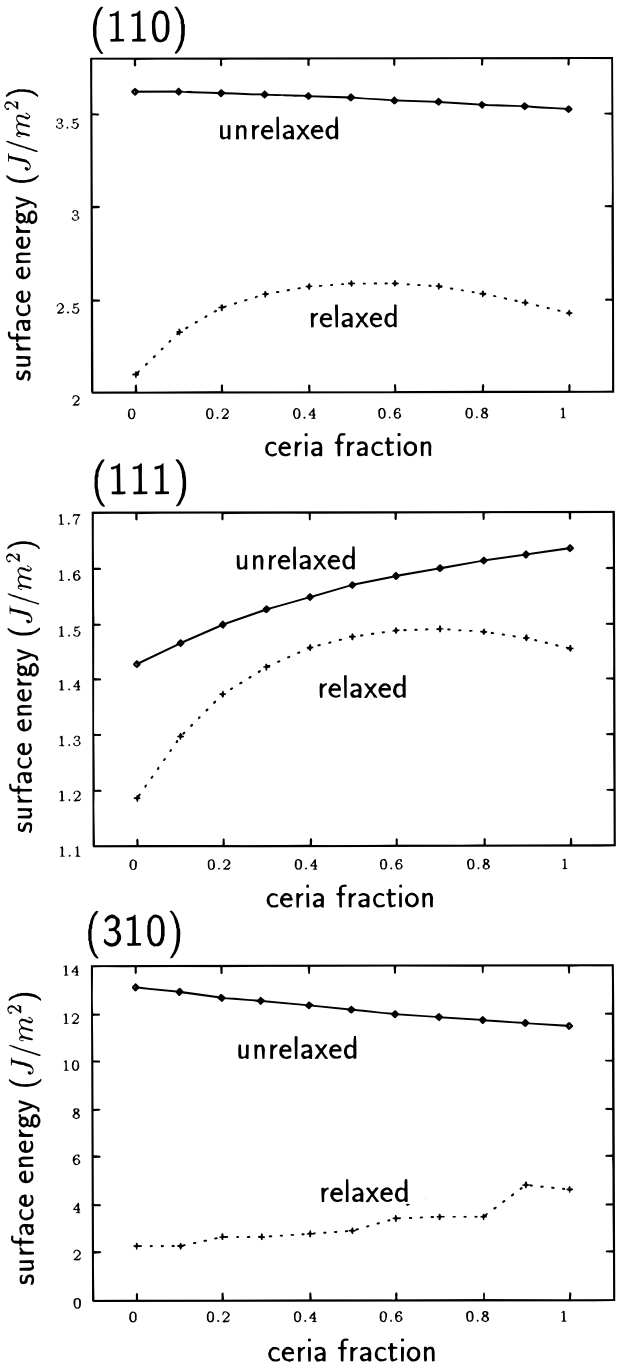

Figure 1. Energy of the (110), (111), and (310) surfaces of CeO_2-ZrO_2 solid solutions as a function of the ceria molar fraction, before and after relaxation.

probably dominate the low-temperature crystal morphology in the absence of dopants or surface irregularities. The same result has been already found in other computational studies of pure ceria.[12,14,15] The relaxed energies of the (110) and (111) surfaces exhibit a maximum at a ceria fraction of about 0.5. Interestingly, the best performance of this material with regard to oxygen storage capacity has been observed on cubic samples having this composition.[28] Since these two surfaces are expected to be present to a great extent in polycrystalline samples, the above correlation may be explained in terms of a higher activity due to a lower stability of the surface. However, it must be noted that the increase in the relaxed surface energy at the 0.5 ceria fraction is not very large suggesting that this could be only one among several factors. The (310) surface of the fluorite

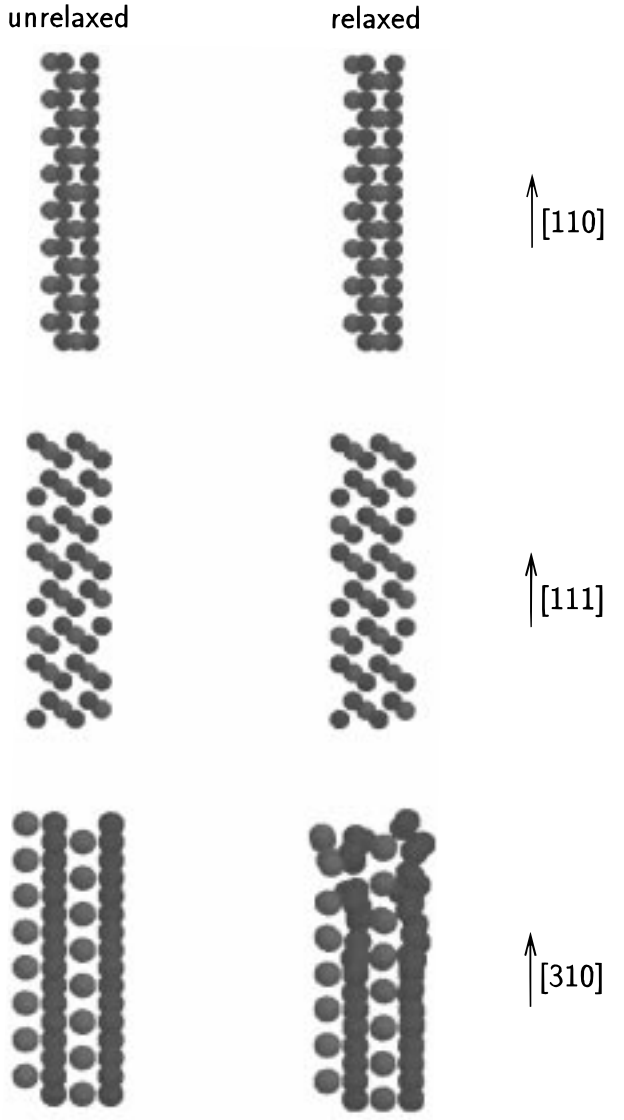

Figure 2. Representative structures, both before and after relaxation, of the (110), (111), and (310) surfaces of the $Ce_{0.5}Zr_{0.5}O_2$ solid solution; light balls are cations, dark balls are oxide ions.

structure is a stepped surface with a high coordinative unsaturation, which explains both the high unrelaxed energy and the large amount of relaxation (Figure 1). Upon energy minimization, this surface undergoes extensive reconstruction (Figure 2): the relaxed energy decreases with increasing zirconia content and reaches values comparable with those of the (110) surface. This can be explained by the smaller ionic size of Zr^{4+} (84 pm) as compared to that of Ce^{4+} (97 pm) together with the preference of zirconium for a lower coordination number. Both factors should relieve the elastic strain in the relaxed surface.

Ce^{4+}/Ce^{3+} Reduction. The redox behavior of the CeO_2-ZrO_2 surfaces was analyzed on the basis of the energetics of the following reaction

$$O_O^{\times} + 2Ce_M^{\times} \rightarrow \frac{1}{2}O_{2(g)} + V_O^{\bullet\bullet} + Ce'_M \qquad (7)$$

where $V_O^{\bullet\bullet}$ represents an oxygen vacancy and Ce'_M a Ce^{3+} state, using Kröger−Vink notation. As previously noted, the transformation of a hybrid cation into a pure Ce^{4+} cation had to be taken into account. The correction is null for pure ceria and increases almost linearly with the zirconia content reaching

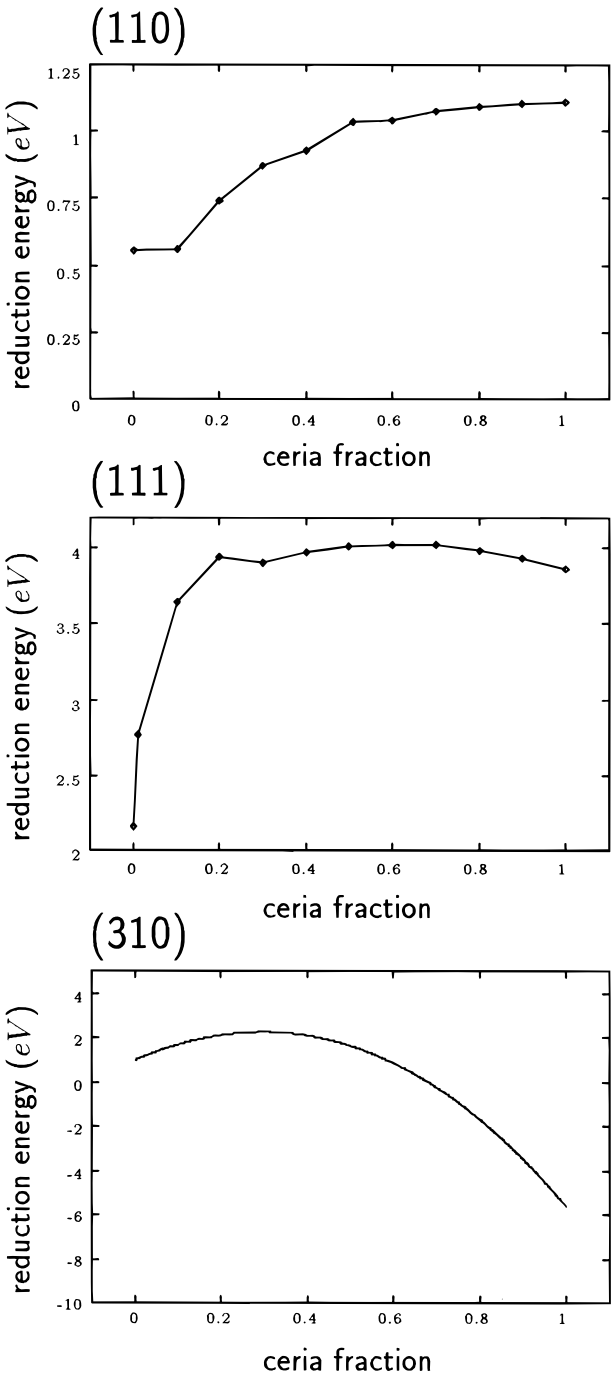

Figure 3. Ce^{4+}/Ce^{3+} reduction energy on the (110), (111), and (310) surfaces of CeO_2-ZrO_2 solid solutions as a function of the ceria fraction.

a value of about 10 eV for pure zirconia. The Ce^{4+}/Ce^{3+} reduction energy on the three surfaces studied in this work was evaluated and results are presented in Figure 3 as a function of the ceria fraction.

The formation of neutral $[Ce'_M-V_O^{\bullet\bullet}-Ce'_M]$ clusters on the relaxed surfaces was considered, so that calculated values include a binding energy term. Figure 3 reveals that an increase in the zirconia content of the solid solution favors the reduction process on both (110) and (111) surfaces. On the latter surface, a sharp decrease is calculated for a zirconia fraction of about 0.8. However, the reduction process is still energetically unfavorable on the (111) surface in comparison with the other surfaces and with the bulk. We note that recent temperature-programmed desorption (TPD) studies on CeO_2 find no significant desorption of oxygen on the (111) surface.[32] It is also worth noting that the reduction energies (≈1.5 eV) from our previous bulk calculations[9] for fractions greater than about 0.1 are not significantly higher than those found here for the (110) surface, while they are lower than the values for the (111) surface. This is consistent with the experimental findings of a large bulk participation in the reduction process during temperature-programmed reduction experiments.[33]

As previously noted, the (310) surface undergoes considerable reconstruction and becomes rather irregular upon relaxation. This irregularity, which has been already pointed out for pure ceria,[14] caused the calculated reduction energy along the whole composition range for the same cluster configuration to be rather scattered. To obtain a qualitative trend, calculations where performed for six different $[Ce'_M-V_O^{\bullet\bullet}-Ce'_M]$ cluster configurations, with the whole set of points fitted to a polynomial function (Figure 3). The behavior of the reduction energy as a function of the composition on this surface seems to be opposite to that found on the (110) and (111) surfaces. At a fixed composition, the reduction energy heavily depends on the particular surface cluster, displaying variations of several electronvolts. This can be interpreted as evidence for a complex topography with a wide variety of different reduction sites, some of which exhibit favorable energies. Considering that at high zirconia contents the (310) surface stability becomes comparable with that of the most stable surfaces (Figure 1), our results suggest that reconstruction with consequent creation of low-energy routes toward Ce^{4+}/Ce^{3+} reduction may be one of the key factors in determining the high oxygen storage capacity observed for these materials. However, we remark that our calculations for the (310) surface are to be taken only on a qualitative level, at least until experimental data become available for comparison.

Oxygen Vacancy Segregation. A key aspect of the Ce^{4+}/Ce^{3+} reduction process in the CeO_2-ZrO_2 solid solutions is the formation of oxygen vacancies (reaction 7). Previous surface modeling work[12,22] has demonstrated the importance of the variation of the defect energy as it penetrates from the surface into the bulk, an effect that can lead to the surface segregation of defects. We have therefore studied the oxygen vacancy energy as a function of the distance from the surface. Results are displayed in Figure 4 for each of the three surfaces studied in this work. As can be seen, there are barriers to the penetration of the oxygen vacancy defect from the surface into the bulk. This suggests that oxygen vacancies tend to segregate to the (110) surface at all compositions, and this tendency increases with decreasing ceria content, for ceria fractions less than about 0.5. The tendency for segregation of the oxygen vacancies on the (111) surface is much less pronounced than that on the (110) surface and also increases, albeit slightly, at smaller ceria fractions.

The energy profiles for the (310) surface were rather scattered as a result of the large reconstruction undergone by this surface; for each composition, the vacancy energies were fitted to piecewise linear functions in order to obtain a smoother surface. In contrast to the two other surfaces, the energy profiles indicate surface segregation of the oxygen vacancies only for high (>0.7) ceria fractions. Relating the above findings to the Ce^{4+}/Ce^{3+} reduction process is not straightforward. First of all, our static calculations give only the energetics, while kinetic contributions to the whole process have to be considered. In our previous study,[9] we found a low activation energy for oxygen vacancy migration indicating rapid oxygen transport through the bulk material. If we assume fast oxygen mobility also in the vicinity of the surface region, then oxygen vacancy migration will be

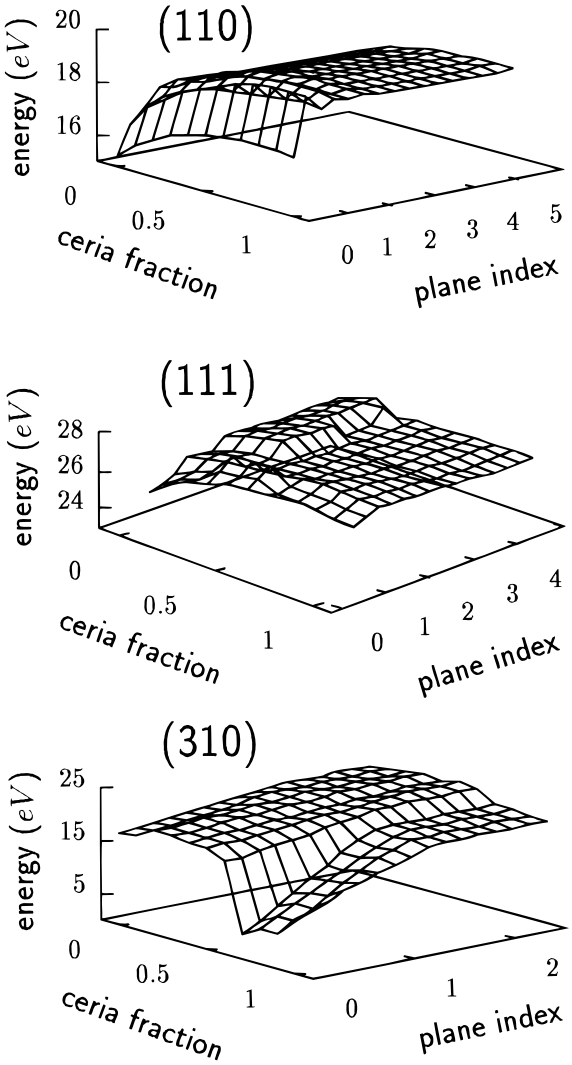

Figure 4. Oxygen vacancy energy as a function of ceria fraction and depth for the (110), (111), and (310) surfaces of CeO_2-ZrO_2 solid solutions. The depth is expressed by the "plane index", defined as the distance from the surface divided by the lattice constant.

thermodynamically controlled. In this context, our results suggest a tendency of the oxygen vacancies to segregate to the most stable (111) and (110) surfaces and that this tendency increases with the zirconia content. This, in turn, would favor bulk reduction by subtracting oxygen vacancies from the bulk and thus driving the reduction equilibrium (equation 7) to the right. However, we recognize that a more detailed mechanism for the Ce^{4+}/Ce^{3+} reduction process has to be assessed before deriving a clear correlation between our calculated energy profiles and experimental results.

Conclusions

Atomistic simulation techniques have been used to probe the surface properties of the CeO_2-ZrO_2 catalysts. We can summarize our conclusions as follows:

(1) The stability order of the surfaces studied in this paper is (111) > (110) > (310), independent of composition; the (310) surface energy steadly decreases with increasing zirconia content, reaching values comparable to the more stable (110) and (111) surfaces.

(2) The (110) and (111) surface energies peak at a ceria fraction of about 0.5, at which a maximum oxygen storage capacity has been experimentally observed for these materials.

(3) The Ce^{4+}/Ce^{3+} reduction energy on the most stable (110) and (111) surfaces is more favorable with increasing zirconia content and becomes comparable with bulk values previously found; this is consistent with results of our temperature-programmed reduction experiments.

(4) Oxygen vacancies tend to segregate to the (110) and (111) surfaces, and this tendency increases with increasing zirconia content in the solid solutions.

Acknowledgment. Ministero dell'Universita' e della Ricerca Scientifica (MURST 40% and 60%), Universita' di Trieste–Relazioni Internazionali, University of Surrey and CNR, Rome, are acknowledged for financial support. G.B. expresses his gratitude to Dr. John Harding, for supplying the simulation codes and giving kind assistance.

References and Notes

(1) Taylor, K. C. Automobile catalytic converters. In *Catalysis—Science and technology*; Anderson, J. R., Boudart, M., Eds.; Springer-Verlag: Berlin, 1984; Vol. 5.
(2) Yao, H. C.; Yu Yao, Y. F. *J. Catal.* **1984**, *86*, 254.
(3) Diwell, A. F.; Rajaram, R. R.; Shaw, H. A.; Truex, T. J. The role of ceria in three-way catalysts. In *Catalysis and automotive pollution control II*; Crucq, A., Ed.; Elsevier: Amsterdam, 1991; Vol. 71.
(4) Harrison, B.; Diwell, A. F.; Hallet, C. *Platinum Metals Rev.* **1988**, *32*, 73.
(5) Oh, S. H. *J. Catal.* **1990**, *124*, 477.
(6) Zamar, F.; Trovarelli, A.; de Leitenburg, C.; Dolcetti, G. *J. Chem. Soc., Chem. Commun.* **1995**, 965.
(7) Balducci, G.; Fornasiero, P.; Di Monte, R.; Kaspar, J.; Meriani, S.; Graziani, M. *Catal. Lett.* **1995**, *33*, 193.
(8) Fornasiero, P.; Balducci, G.; Di Monte, R.; Kaspar, J.; Sergo, V.; Gubitosa, G.; Ferrero, A.; Graziani, M. *J. Catal.* **1996**, *164*, 173.
(9) Balducci, G.; Kaspar, J.; Fornasiero, P.; Graziani, M.; Islam, M. S.; Gale, J. D. *J. Phys. Chem. B* **1997**, *101*, 1750.
(10) Butler, V.; Catlow, C. R. A.; Fender, B. E. F.; Harding, J. H. *Solid State Ionics* **1983**, *8*, 109.
(11) Adler, S. B.; Smith, J. W. *J. Chem. Soc., Faraday Trans.* **1993**, *89*, 3123.
(12) Sayle, T. X. T.; Parker, S. C.; Catlow, C. R. A. *Surf. Sci.* **1994**, *316*, 329.
(13) Sayle, T. X. T.; Parker, S. C.; Catlow, C. R. A. *J. Phys. Chem.* **1994**, *98*, 13625.
(14) Conesa, J. C. *Surf. Sci.* **1995**, *339*, 337.
(15) Cordatos, H.; Ford, D.; Gorte, R. J. *J. Phys. Chem.* **1996**, *100*, 18128.
(16) Mackrodt, W. C.; Woodrow, P. M. *J. Am. Ceram. Soc.* **1986**, *69*, 277.
(17) Dwivedi, A.; Cormack, A. N. *Philos. Mag. A* **1990**, *61*, 1.
(18) Cormack, A. N.; Parker, S. C. *J. Am. Ceram. Soc.* **1990**, *73*, 3220.
(19) Stefanovich, E. V.; Shluger, A. L.; Catlow, C. R. A. *Phys. Rev. B* **1994**, *49*, 11560.
(20) Wilson, M.; Schönberg, U.; Finnis, M. W. *Phys. Rev. B* **1996**, *54*, 9147.
(21) Harding, J. H. *Rep. Prog. Phys.* **1990**, *53*, 1403.
(22) Colbourn, E. A. *Surf. Sci. Rep.* **1992**, *15*, 281.
(23) Dick, B. G.; Overhauser, A. W. *Phys. Rev.* **1958**, *112*, 90.
(24) Harding, J. H. A guide to MIDAS—A program for studying surfaces and interfaces in ionic crystals. Harwell Report, AERE-R13127, 1988.
(25) Mott, N. F.; Littleton, M. J. *Trans. Faraday Soc.* **1938**, *34*, 485.
(26) Lidiard, A. B. *J. Chem. Soc., Faraday Trans.* **1989**, *85*, 341.
(27) Duffy, D. M.; Tasker, P. W. CHAOS: Computer simulation HAdes on Surfaces. Harwell Report, AERE-R11059, 1983.
(28) Fornasiero, P.; Di Monte, R.; Ranga Rao, G.; Kaspar, J.; Meriani, S.; Graziani, M. *J. Catal.* **1995**, *151*, 168.
(29) Chiodelli, G.; Flor, G.; Scagliotti, M. *Solid State Ionics* **1996**, *91*, 109.
(30) Tasker, P. W. *J. Phys. C: Solid State Phys.* **1979**, *12*, 4977.
(31) Sotiropoulou, D.; Nikolopoulos, P. *J. Mater. Sci.* **1991**, *26*, 1395.
(32) Putna, E. S.; Vohs, J. M.; Gorte, R. J. *J. Phys. Chem.* **1996**, *100*, 17862.
(33) Ranga Rao, G.; Kaspar, J.; Di Monte, R.; Meriani, S.; Graziani, M. *Catal. Lett.* **1994**, *24*, 107.